Published in final edited form as:
J Magn Reson Imaging. 2012 May ; 35(5): 1125–1132. doi:10.1002/jmri.23545.

Simultaneous Field and R_2* Mapping to Quantify Liver Iron Content Using Autoregressive Moving Average Modeling

Brian A. Taylor, Ph.D.[1], **Ralf B. Loeffler, Ph.D.**[1], **Ruitian Song, Ph.D.**[1], **Mary E. McCarville, M.D.**[1], **Jane S. Hankins, M.D., M.S.**[2], and **Claudia M. Hillenbrand, Ph.D.**[1]

[1]Department of Radiological Sciences, St. Jude Children's Research Hospital, Memphis, Tennessee

[2]Department of Hematology, St. Jude Children's Research Hospital, Memphis, Tennessee

Abstract

Purpose—To investigate the use of a complex multi-gradient echo (mGRE) acquisition and an autoregressive moving average (ARMA) model for simultaneous susceptibility and R_2* measurements for the assessment of liver iron content (LIC) in patients with iron overload.

Materials and Methods—Fifty MR exams with magnitude and phase mGRE images are processed using the ARMA model which provides fat-separated field maps, R_2* maps, and T_1-W imaging. The LIC is calculated by measuring the susceptibility between the liver and the right transverse abdominal muscle from the field maps. The relationship between LIC derived from susceptibility measurements and LIC from R_2* measurements is determined using linear least squares regression analysis.

Results—LIC measured from R_2* is highly correlated to the LIC from the susceptibility method (mg/g dry = 8.99 ± 0.15 × (mg Fe/ml of wet liver) −2.38 ± 0.29, R^2=0.94). The field inhomogeneity in the liver is correlated with R_2* (R^2=0.85).

Conclusion—By using the ARMA model on complex mGRE images, both susceptibility and R_2*-based LIC measurements can be made simultaneously. The susceptibility measurement can be used to help verify R_2* measurements in the assessment of iron overload.

Keywords

iron overload; liver; R_2* mapping; susceptibility; multi-gradient echo (mGRE); autoregressive moving average (ARMA) modeling

Introduction

Patients with hematologic disorders such as *β*-thalassemia major and sickle cell disease often require chronic blood transfusions for disease management. Although this reduces the primary disease burden, a common side effect is the accumulation of iron in many organs including the liver (1-5). Excessive iron accumulation also occurs in disorders such as hereditary hemochromatosis (6). It is imperative to monitor the amount of iron in the liver because significant conditions such as liver cirrhosis and hepatocellular carcinoma can develop as a result of iron overload due to increased oxidative stress and generation of free radicals (7).

Correspondence: Claudia M. Hillenbrand, Ph.D. Department of Radiological Sciences, St. Jude Children's Research Hospital, 262 Danny Thomas Blvd. MS 220, Memphis, TN 38105, Phone: 901-595-4118, Fax: 901-595-3981, claudia.hillenbrand@stjude.org.

Hepatic iron overload has traditionally been monitored by measuring the liver iron content (LIC) by needle biopsy. However, the procedure is invasive and painful with a risk of complications such as infection and bleeding (8). This has led to the development of noninvasive methods that can be performed at a greater frequency than liver biopsy procedures. One noninvasive method is to measure the apparent spin–spin relaxation rate (R_2*) of liver tissue with multi-gradient echo (mGRE) magnetic resonance imaging (1,9-17). Iron compounds increase the macroscopic susceptibility, thereby increasing the R_2* value in tissue, where it is present in excess. This method has been calibrated with liver biopsies, making it a useful indirect method to quantify LIC (10,11).

A less common method to measure LIC is susceptometry (18-20). This method, typically performed by a superconducting quantum interference device (SQUID), has also been calibrated with biopsy, but the cost of the equipment has limited its clinical use. Some studies have also used MR to measure the susceptibility via field mapping as an additional acquisition to the mGRE acquisition (21-23). LIC values may be more accurately estimated by susceptometry methods than by R_2* methods, as the former is a direct measure of susceptibility due to iron content (21). However, the absolute phase for MR susceptometry methods is difficult to obtain because of factors such as flow, motion, and phase variations (22).

In this work, we investigated an autoregressive moving average (ARMA) model (24-26) of a mGRE MR acquisition, which is a method that can map the R_2*, in addition to the magnetic field, by using magnitude and phase data from a single mGRE acquisition for the purpose of LIC quantification. We used this model in forty-five patients and five volunteers to make susceptibility measurements at the interface of the liver and the surrounding non-fatty tissue, and convert these measurements to LIC using Curie's law (27). Susceptibility measurements were correlated to the iron concentrations derived from R_2* values in the liver as previously described (11). By using the ARMA model on the same mGRE acquisition, R_2* and susceptibility measurements can be made simultaneously – thereby providing an additional measurement to aid in the quantitative assessment of iron overload. This additional susceptibility measurement can reduce measurement error by assuring that patients with liver R_2* values within the mild to severe iron overload range indeed have a correct assessment of elevated LIC – particularly at mild levels (0.5 – 2.0 mg/g wet liver weight) where decisions on initiation or cessation of therapy, such as chelation, are typically made. This new method can allow differentiation from other hepatic disease processes, such as fibrolamellar lesions, fatty infiltration, primary liver malignancies, metastases, and tissue necrosis, all of which can increase R2* values in the liver in the absence of elevated LIC, potentially confounding liver iron quantification (28).

Materials and Methods

Simultaneous R_2* and Field Mapping with an Autoregressive Moving Average (ARMA) Model

The mGRE signal consisting of *N* chemical shifts, *x(TE)*, can be modeled discretely as a function of the echo-time (TE) as

$$x(TE) = \sum_{k=1}^{N} C_k e^{-\left(2\pi i f_k + R^*_{2,k}\right)TE} + w(TE) \quad [1]$$

where C_k is the complex amplitude, f_k is the proton resonant frequency (PRF) and $R_{2,k}$* is the apparent spin-spin relaxation rate of each chemical shift and *w(TE)* is white noise with

zero mean. Using the *z*-transform, equation [1] can be described as a multi-peak autoregressive moving average (ARMA) process as

$$X(z)=\frac{B(z)}{A(z)}=\frac{\sum_{k=0}^{N-1}\beta_k z^{-k}}{1+\sum_{k=1}^{N}\alpha_k z^{-k}}, \quad [2]$$

where *z* is a complex number (24-26). Equation [2] can be expanded to several poles to measure chemical shifts as seen in previous studies, which is very useful when lipids are present (29).

To calculate the coefficients α_k and β_k, a set of over-determined equations need to be solved. We used an approach based on Prony's method (25) and the iterative Steiglitz-McBride (SM) algorithm (30), as done in an ARMA-based approach for MR temperature imaging (31). Both algorithms are used in applications such as digital filter design and communications (25). The advantages of using these algorithms are that they require minimal interaction by the user (32), exhibit relatively fast processing times (31), and perform robustly in the presence of noise (30,33).

After calculating the coefficients α_k and β_k, the poles can be calculated as roots of the denominator in equation [2]. If ρ_k denotes a pole for a chemical shift such as water or lipid, then the PRF (in ppm) can be expressed as

$$f_k=-\frac{\mathrm{Im}[\ln(\rho_k)]}{2\pi\cdot\Delta TE\cdot\gamma B_0}, \quad [3]$$

where γ is the gyromagnetic ratio and B_0 is the applied magnetic flux density. In addition, the R_2* value for each chemical shift can be expressed as

$$R^*_{2,k}=-\frac{\mathrm{Re}[\ln(\rho_k)]}{\Delta TE}. \quad [4]$$

Finally, the complex amplitude can be computed separately by using the Cauchy's Residue Theorem where

$$C_k=\frac{B(\rho_k)}{A'(\rho_k)} \quad [5]$$

and

$$A'(z^{-1})=\frac{dA(z^{-1})}{dz^{-1}}. \quad [6]$$

Susceptometry from ARMA-Calculated Field Maps

Ignoring effects from field inhomogeneity, which in the liver of a healthy subject is on the order of 0.1-0.2 ppm/cm (34), the susceptibility Δχ is calculated from the field map by

$$\Delta\chi = \frac{3\Delta f}{2\pi\left(1 - 3\cos^2\theta + S_{hf}\right)} \quad [7]$$

where Δf is the mean change in the field between two regions, θ is the angle between the field measurement and the static field (θ was set to 90° in this work since all images were acquired in the transverse plane), and S_{hf} is the orientation-independent shift term set to −0.133 from results of previous studies (21,35,36). Also note that the change in phase, $\Delta\phi$, can be used with an image at TE where

$$\Delta\phi = \Delta f \cdot TE \quad [8]$$

Derived from Curie's law, the susceptibility of η iron atoms at temperature T (in Kelvin), inside the volume V with the magnetic moment $p\mu_B$ is

$$\Delta\chi = \mu_0 \frac{\eta}{V} \frac{(p\mu_B)^2}{3kT} \quad [9]$$

where μ_0 is the magnetic permeability in a vacuum and k is the Boltzmann constant. Knowing the atomic weight of iron, equation [8] can be used to measure the iron concentration [Fe] by

$$[Fe] = \frac{\Delta\chi \cdot T}{\left(2.81x10^{-5}\frac{ml \cdot K}{mg}\right)p^2}, \quad [10]$$

where p=4 Bohr magneton for iron in human liver at T=310 K (19). So at body temperature,

$$[Fe] = \frac{\Delta\chi}{1.45x10^{-6}\frac{ml}{mg}} \quad [11]$$

Therefore, by using equations [7] and [11], the field map can be used to estimate the concentration of iron in milligram per milliliter of wet weight liver (27).

MR Imaging and Analysis

Forty-five MR exams (22 male/23 female, mean age = 15.3 years, range = 3 – 42 years) with magnitude and phase mGRE images were retrospectively analyzed under an Institutional Review Board-approved protocol. These patients all have histories of receiving blood transfusions as part of their therapy. Twenty-three were diagnosed with sickle cell disease and ten were diagnosed with β-thalassemia major. The twelve others were diagnosed with conditions that required multiple blood transfusions and/or bone marrow transplantation including acute lymphoblastic leukemia (n=3), hemoglobin H disease (n=2), congenital dyserythropoietic anemia (n=2), acute myeloid leukemia (n=1), small cell carcinoma (n=1),hypogammaglobulinemia (n=1), aplastic anemia (n=1) and β-thalassemia intermedia (n=1). Five volunteers (2 male/3 female, mean age = 45.6 yrs, range: 20 – 58 yrs) with no history of blood transfusions, or hereditary hemochromatosis also underwent scans. Informed consent was obtained for all exams. All subjects were scanned on 1.5T whole body scanners (Siemens, Malvern, PA) with a phased-array body coil. A single breath-hold technique was used to obtain mGRE axial images with a repetition time of 200 ms. Echo

times ranged from 0.9 ms to 28.5 ms at increments of 1.1 to 1.4 ms (echo train length=20). Other imaging parameters were as follows: flip angle 25°, slice thickness 10 mm, in-plane resolution 3.125 mm^2, matrix size 128 × (96–128) and field of view 380 mm × (285 mm–380 mm). Total acquisition time for the 20 slices ranged from 18 to 25 sec.

To compare T_2* values between the ARMA technique and a typical non-linear least squares (NLS) technique, in each patient an ROI was placed in the liver, which did not include the hepatic vessels. The T_2* was calculated with the ARMA method and a NLS technique as previously described by Hankins et al (11). The root mean squared difference was calculated between each method.

PRF maps were also generated by using the ARMA model. For LIC measurements by susceptometry, two ROIs were drawn from the field map: one in the right lateral side of the liver and the other in the adjacent right transverse abdominal muscle. The mean and standard deviation (SD) of the PRF values in the ROIs were recorded. The susceptibility values obtained between these ROIs were used to calculate the iron concentration in milligram per gram of wet weight liver. These concentrations were correlated to LIC in milligram Fe per gram of dry weight liver by using the mean R_2* from the ROI in the liver (11). A regression line was calculated between the iron concentration measurements from these two methods by using linear least squares regression analysis. In one case, fibrosis was diagnosed by a clinically-indicated liver biopsy two weeks after MR scanning. This case was excluded from the regression analysis because of the known variability in iron measurements from fibrotic liver tissue (15) and because R_2* effects occur due to fibrosis with or without the presence of iron (10,37).

In the forty-nine cases with no documented evidence of pathologies that can be present without excessive LIC like fibrosis or cirrhosis, an ROI was drawn around the periphery of the entire liver in one axial slice. Vessels within the liver parenchyma were excluded from the ROI as previously described (38). The field inhomogeneity was calculated by the standard deviation of the PRF measurements in the liver. This was correlated to the whole-liver R_2* value by using linear least squares regression analysis.

Results

In all patients, the root mean squared difference between the ARMA-calculated T2* fit and NLS fit in ROIs in the liver was 0.08 ms (p=0.27). For example, in the patient in figure 1, the difference in the T2* maps between ARMA and NLS was less than 0.3 ms within the liver parenchyma, excluding vessels. While at the same time, there was high contrast in the liver on the ARMA-calculated field map when compared to the adjacent soft tissue to indicate the presence of iron in the liver.

On the field maps generated by the ARMA model, the magnetic susceptibility difference between the liver and the adjacent abdominal muscle tissue increased with increasing R_2* (decreasing T_2*; see figure 2). Figures 2a and 2c demonstrate that in the volunteers, there was little contrast (~0.1 ppm) between the adjacent tissue parenchyma and the liver in the field maps. However, the distinction of the field map between the liver and adjacent soft tissue was clear in images of iron-overloaded patients with low T_2*. Figures 2b and 2d show an example from a patient with a whole-liver R_2* that corresponded to an iron concentration of 16.5 ± 2.2 mg Fe/g dry liver (11). The susceptibility was $3.20 \times 10^{-6} \pm 0.43 \times 10^{-6}$ between the right lateral side of the liver and the adjacent transverse abdominal muscle, and this value was approximately 27.8 times of that of the field map of the volunteer in figure 2a ($1.15 \times 10^{-7} \pm 0.05 \times 10^{-7}$).

Figure 3 shows a plot of the iron concentration from the ROI-based R_2* method and the susceptibility method. Even at very high R_2* values (> 500 Hz), the dry liver iron concentration from the R_2* method was highly correlated to the wet liver weight from the susceptibility method (R^2=0.94, p<0.0001). The slope of the regression line was 8.99 ± 0.15 mg Fe/g dry liver per mg Fe/ml of wet liver, with an intercept of −2.38 ± 0.29 mg Fe/g dry liver. Among the patient subjects, the difference in the PRF between the two ROIs ranged from 0.09 to 3.69 ppm ($\Delta\chi$=1.61 × 10^{-7} to 6.68 × 10^{-6}) with a mean of 1.33 ppm ($\Delta\chi$=2.40×10^{-6}). The range in the volunteers was 0.06 to 0.27 ppm ($\Delta\chi$=1.15 × 10^{-7} to 4.79 × 10^{-7}) with a mean of 0.17 ppm ($\Delta\chi$=3.10 × 10^{-7}).

Throughout the entire liver, the variation of PRF values was associated with the whole-liver mean R_2* value. Figure 4 is a plot of the standard deviation of the PRF values in the liver to the whole-liver R_2*. The slope was 0.0012 ± 0.0005 ppm/Hz with an intercept of 0.15 ± 0.26 ppm (R^2=0.85, p<0.0001). There was a wider distribution of PRF values in the cases with high whole-liver R_2* values (> 500 Hz), demonstrating a larger field gradient throughout the liver as LIC increases.

The case that was excluded from the study due to biopsy-confirmed fibrosis is shown in figure 5. The T_2* values ranged from approximately 2.8 ms to 31.9 ms at certain areas near the portal vein. Qualitatively, the field map was relatively homogenous with no obvious shift in the field at the liver. An ROI was taken in a low T_2* area and LIC measurements were measured with the susceptibility and T_2* methods. Using the T_2*, the LIC was approximated at 3.56 ± 0.43 mg Fe/g dry liver. Using the susceptibility method described above, the susceptibility-based LIC was 0.29 ± 0.08 mg Fe/g wet liver, which demonstrates that very little iron is present. By converting the dry liver LIC to wet liver LIC, the 95% confidence interval of the T_2* measurement was 0.58 to 0.75 mg Fe/g wet liver weight. This means that the susceptibility method is measuring a lower LIC when compared quantitatively to the T_2*(R_2*) calibration method. The biopsy confirmed only trace amounts of iron.

Discussion

We used an ARMA model to calculate the susceptibility induced from LIC in patients with iron overload by using phase and magnitude data from standard mGRE acquisitions, which are being more frequently used for R_2*-based iron concentration measurements. By incorporating the infrequently-used phase imaging from the acquisition, field maps and R_2* maps can be generated by using the ARMA model without requiring additional imaging time. A complementary field map with shifts in the PRF in the liver in addition to high R_2* measurements should increase the confidence when excessive amounts of iron are present in the liver. In practice, one can use the T_2* (R_2*) map to quantify LIC from a validated calibration curve using the same acquisition parameters as done in the calibration (10,11). Then, one can measure the susceptibility between the liver and transverse abdominal muscle using the field map to help verify if there is indeed increased susceptibility due to excess iron.

As shown in figure 5, T_2* can decrease due to a variety of causes– thus possibly overestimating the amount of iron present. In this particular case, a biopsy showed evidence of fibrosis with only trace amounts of iron. While large variations in T_2* can point to focal diseases like fibrosis, the field map can possibly aid in determining if iron is also a contributing factor in the T_2* change. The advantage of the field map in these cases is that conditions like fibrosis and steatosis have a lower susceptibility effect (on the order of one magnitude) when compared to the presence of iron in the liver (39). This makes susceptibility measurements from the field map highly specific to LIC. Therefore, we

propose that a simple test to check that if the susceptibility-based LIC between the transverse abdominal muscle and adjacent liver is below the 95% confidence interval on the R_2* vs susceptibility LIC calibration curve, then the change in R_2* may not be entirely due to iron content and the LIC results have to be reported with caution. Also, this test is just as important in cases where LIC values follow the calibration since it should increase the confidence that accurate LIC estimations are obtained. In the case in figure 5, the susceptibility is below the 95% confidence interval given the R_2* values measured thereby showing that pathology other than iron may be causing the discrepancy between LIC and R_2*.

We calculated susceptibility-based measurements in milligram per gram of wet liver, as in other susceptibility studies (18-20). The ratio between dry and wet liver (mg/g dry = 8.99 ± 0.15 × (mg Fe/ml of wet liver) −2.38 ± 0.29, ratio = 7.95) was higher than what has been reported previously. Recently, there has been debate regarding this ratio, since the commonly used ratio of 3.33 has not been thoroughly validated in the literature (40); some studies have reported a ratio of at least 5.5 ± 1.0 (41-43). This value is also dependent on the biopsy and the tissue-processing technique used (40). The ability to measure both susceptibility and R_2* simultaneously with and compared to biopsy measurements may help determine whether this value is consistent and whether direct conversions from wet to dry liver weights can be appropriately made. It is important to note that there can be a small susceptibility difference between the liver and adjacent soft tissue. This may slightly overestimate the wet liver LIC values and may explain the lower the value of the y-intercept in the calibration in figure 3.

This concept of using susceptometry and R_2* together is similar to the work of Wang et al (21), which incorporated susceptibility and R_2* for cardiac iron assessment. They also validated the susceptometry technique across different platforms using a highly-controlled phantom study. For susceptibility measurements, 3D gradient echo imaging was used in addition to R_2* mapping from a multi-gradient echo acquisition. This work differs in that the field map is generated from the multi-gradient echo data used for R_2* mapping and the ARMA model – thereby decreasing the needed imaging time to make these measurements.

In areas of low SNR caused by high LIC, ARMA methods may give spurious results seen as large variations in the PRF values both above and below the PRF on non-iron loaded tissue (26). However, even at very high LIC concentrations (≥ 20 mg/g dry weight liver determined by high R_2* values), estimates in the liver provide consistently lower PRF values (positive susceptibility) indicating the presence of iron, thereby supporting the reliability of these measurements. However, measurements are less precise with higher LIC estimates (Figs. 3 and 4). As shown in Cramer-Rao lower bound analysis (26), the lower the T_2* and SNR, the higher the uncertainty in the measurements.

On a note on the acquisition technique, mGRE acquisitions can run monopolar or bipolar frequency encoding gradients. Bipolar gradients can be used to lower the TE values, which can be advantageous especially in tissues with low T_2*. However, phase images arising from the negative and positive polarity gradients must be closely monitored. Timing errors between positive and negative polarity gradients can manifest as N/2 ghosts, as these errors cause phase shifts between the positive and negative gradients (31,44). This can be corrected by measuring the offset between the odd and even echoes and then multiplying the phase offset by either the odd or even echoes.

Very similar T_2* values are measured with the ARMA and NLS techniques, thereby lending validity to these measurements even in the presence of field inhomogenities directly measured by the ARMA technique. Lipid content in the liver was not detected from this

patient population comprising mainly of children with sickle cell disease, but the ARMA technique can also take lipid into account to separately calculate water and lipid R_2* values (26,31) making the technique very useful for patients with steatosis. Recent work has been reported on iterative water-lipid decomposition with R_2* estimation in the presence of lipid (9,13). ARMA differs from these iterative decomposition methods in R_2* estimation by calculating different R_2* values for each chemical shift instead of calculating one R_2* for the voxel (9,13). Also in these studies, the signal model is constrained to assume certain relative chemical shifts (i.e. the distance between water and lipid in a spectrum). We have shown that the water chemical shift can change due to iron content and this may affect the lipid chemical shift as well. Future work should investigate these susceptibility effects when lipid is present at least at the mg/ml range of iron content as seen in patients with iron overload to assure that the shifts due to high LIC do not adversely affect the fat fraction estimation. At the μg/ml range, Yu et al. (13) and Lee et al. (12) showed that the fat-fraction can be determined by similar multi-echo techniques. At these ranges, the susceptibility may not be high enough to affect the chemical shift of water and lipid. For example, by using equations [7] and [10], ten μg/ml of iron will change the field by only 0.008 ppm.

A limitation of this study is that biopsies were not performed and therefore we cannot make direct correlation to iron concentrations. Also, without biopsies the accuracy of the susceptibility measurements of LIC compared to R_2*-LIC measurements cannot be determined. However, when using R_2* measurements as an indirect measurement of LIC from a calibrated technique with identical acquisition parameters (11), the susceptibilities measured from the field maps correlated highly with LIC – thereby indicating that our susceptibility-based measurement for LIC is reliable.

In conclusion, using an autoregressive moving average model, complex mGRE data was processed to create R_2* and field maps – thereby providing two simultaneous measurements for LIC. The LIC measurements from both susceptometry and the R_2* method were strongly associated (R^2=0.94). The presence of iron, determined by whole-liver R_2* measurements, also increased the field inhomogeneity in the liver (R^2=0.85). Given the strength of the association between these two techniques, the use of the field map in addition to R_2* can provide an additional quantitative assessment of LIC to aid in the diagnosis of liver iron overload and/or monitor treatment response.

Acknowledgments

The authors would like to thank Vani Shanker, Ph.D., for the scientific editing of this manuscript.

Funding Support: NIH 5RO1DK088988-02 and American Lebanese Syrian Associated Charities (ALSAC)

References

1. Taher AT, Musallam KM, Inati A. Iron overload: consequences, assessment, and monitoring. Hemoglobin. 2009; 33 1:S46–57. [PubMed: 20001632]
2. Olivieri NF. Progression of iron overload in sickle cell disease. Semin Hematol. 2001; 38(1 Suppl 1):57–62. [PubMed: 11206962]
3. Harmatz P, Butensky E, Quirolo K, Williams R, Ferrell L, Moyer T, Golden D, Neumayr L, Vichinsky E. Severity of iron overload in patients with sickle cell disease receiving chronic red blood cell transfusion therapy. Blood. 2000; 96(1):76–79. [PubMed: 10891433]
4. Prati D, Maggioni M, Milani S, Cerino M, Cianciulli P, Coggi G, Forni GL, Magnano C, Meo A, Gramignoli R, Rebulla P, Fiorelli G, Cappellini MD. Clinical and histological characterization of liver disease in patients with transfusion-dependent beta-thalassemia. A multicenter study of 117 cases. Haematologica. 2004; 89(10):1179–1186. [PubMed: 15477201]

5. Brittenham GM. Iron-chelating therapy for transfusional iron overload. N Engl J Med. 2011; 364(2): 146–156. [PubMed: 21226580]
6. Olynyk JK, St Pierre TG, Britton RS, Brunt EM, Bacon BR. Duration of hepatic iron exposure increases the risk of significant fibrosis in hereditary hemochromatosis: a new role for magnetic resonance imaging. Am J Gastroenterol. 2005; 100(4):837–841. [PubMed: 15784029]
7. Kohgo Y, Ikuta K, Ohtake T, Torimoto Y, Kato J. Body iron metabolism and pathophysiology of iron overload. Int J Hematol. 2008; 88(1):7–15. [PubMed: 18594779]
8. Angelucci E, Baronciani D, Lucarelli G, Baldassarri M, Galimberti M, Giardini C, Martinelli F, Polchi P, Polizzi V, Ripalti M, et al. Needle liver biopsy in thalassaemia: analyses of diagnostic accuracy and safety in 1184 consecutive biopsies. Br J Haematol. 1995; 89(4):757–761. [PubMed: 7772512]
9. Vasanawala SS, Yu H, Shimakawa A, Jeng M, Brittain JH. Estimation of liver T*(2) in transfusion-related iron overload in patients with weighted least squares T*(2) IDEAL. Magn Reson Med. 2011
10. Wood JC, Enriquez C, Ghugre N, Tyzka JM, Carson S, Nelson MD, Coates TD. MRI R2 and R2* mapping accurately estimates hepatic iron concentration in transfusion-dependent thalassemia and sickle cell disease patients. Blood. 2005; 106(4):1460–1465. [PubMed: 15860670]
11. Hankins JS, McCarville MB, Loeffler RB, Smeltzer MP, Onciu M, Hoffer FA, Li CS, Wang WC, Ware RE, Hillenbrand CM. R2* magnetic resonance imaging of the liver in patients with iron overload. Blood. 2009; 113(20):4853–4855. [PubMed: 19264677]
12. Lee SS, Lee Y, Kim N, Kim SW, Byun JH, Park SH, Lee MG, Ha HK. Hepatic fat quantification using chemical shift MR imaging and MR spectroscopy in the presence of hepatic iron deposition: validation in phantoms and in patients with chronic liver disease. J Magn Reson Imaging. 2011; 33(6):1390–1398. [PubMed: 21591008]
13. Yu H, McKenzie CA, Shimakawa A, Vu AT, Brau AC, Beatty PJ, Pineda AR, Brittain JH, Reeder SB. Multiecho reconstruction for simultaneous water-fat decomposition and T2* estimation. J Magn Reson Imaging. 2007; 26(4):1153–1161. [PubMed: 17896369]
14. Wu EX, Kim D, Tosti CL, Tang H, Jensen JH, Cheung JS, Feng L, Au WY, Ha SY, Sheth SS, Brown TR, Brittenham GM. Magnetic resonance assessment of iron overload by separate measurement of tissue ferritin and hemosiderin iron. Ann N Y Acad Sci. 2010; 1202:115–122. [PubMed: 20712781]
15. Anderson LJ, Holden S, Davis B, Prescott E, Charrier CC, Bunce NH, Firmin DN, Wonke B, Porter J, Walker JM, Pennell DJ. Cardiovascular T2-star (T2*) magnetic resonance for the early diagnosis of myocardial iron overload. Eur Heart J. 2001; 22(23):2171–2179. [PubMed: 11913479]
16. Roghi A, Cappellini MD, Wood JC, Musallam KM, Patrizia P, Fasulo MR, Cesaretti C, Taher AT. Absence of cardiac siderosis despite hepatic iron overload in Italian patients with thalassemia intermedia: an MRI T2* study. Annals of hematology. 2010; 89(6):585–589. [PubMed: 20016898]
17. Musallam KM, Taher AT. Deferiprone or deferasirox for cardiac siderosis in beta-thalassemia major. Haematologica. 2011; 96(2):e5–6. author reply e7-8. [PubMed: 21282714]
18. Carneiro AA, F JP, Zago MA, Covas DT, Angulo IL, Baffa O. AC superconductor susceptometric system to evaluate liver iron overload. Rev Sci Instrum. 2003; 74:2098–3103.
19. Marinelli M, Gianesin B, Balocco M, Beruto P, Bruzzone C, Carrara P, Gallusi P, Macco A, Musso M, Oliveri E, Pelucchi S, Sobrero G, Villa R, Forni GL. Total iron-overload measurement in the human liver region by the magnetic iron detector. IEEE Trans Biomed Eng. 2010; 57(9): 2295–2303. [PubMed: 20562030]
20. Brittenham GM, Farrell DE, Harris JW, Feldman ES, Danish EH, Muir WA, Tripp JH, Bellon EM. Magnetic-susceptibility measurement of human iron stores. N Engl J Med. 1982; 307(27):1671–1675. [PubMed: 7144866]
21. Wang ZJ, Fischer R, Chu Z, Mahoney DH Jr, Mueller BU, Muthupillai R, James EB, Krishnamurthy R, Chung T, Padua E, Vichinsky E, Harmatz P. Assessment of cardiac iron by MRI susceptometry and R2* in patients with thalassemia. Magn Reson Imaging. 2010; 28(3):363–371. [PubMed: 20061110]

22. Chu Z, Cohen AR, Muthupillai R, Chung T, Wang ZJ. MRI measurement of hepatic magnetic susceptibility-phantom validation and normal subject studies. Magn Reson Med. 2004; 52(6): 1318–1327. [PubMed: 15562494]
23. Holt RW, Diaz PJ, Duerk JL, Bellon EM. MR susceptometry: an external-phantom method for measuring bulk susceptibility from field-echo phase reconstruction maps. J Magn Reson Imaging. 1994; 4(6):809–818. [PubMed: 7865941]
24. Belkic D, Belkic K. The fast Pade transform in magnetic resonance spectroscopy for potential improvements in early cancer diagnostics. Phys Med Biol. 2005; 50:4385–4408. [PubMed: 16148400]
25. Jackson, LB. Digital Filters and Signal Processing with Matlab Exercises. Norwell, MA., editor. Kulwer Academic Publishers; 1996. p. 502
26. Taylor BA, Hwang KP, Hazle JD, Stafford RJ. Autoregressive moving average modeling for spectral parameter estimation from a multigradient echo chemical shift acquisition. Med Phys. 2009; 36(3):753–764. [PubMed: 19378736]
27. Allen PD, St Pierre TG, Chua-anusorn W, Strom V, Rao KV. Low-frequency low-field magnetic susceptibility of ferritin and hemosiderin. Biochim Biophys Acta. 2000; 1500(2):186–196. [PubMed: 10657588]
28. Curvo-Semedo L, Brito JB, Seco MF, Costa JF, Marques CB, Caseiro-Alves F. The hypointense liver lesion on T2-weighted MR images and what it means. Radiographics. 2010; 30(1):e38. [PubMed: 19901085]
29. Taylor BA, Elliott AM, Hwang KP, Shetty A, Hazle JD, Stafford RJ. Measurement of temperature dependent changes in bone marrow using a rapid chemical shift imaging technique. J Magn Reson Imaging. 2011; 33(5):1128–1135. [PubMed: 21509871]
30. Steiglitz K, McBride L. A technique for the identification of linear systems. IEEE Transactions on Automatic Control. 1965; 10(4):461–464.
31. Taylor BA, Hwang KP, Elliott AM, Shetty A, Hazle JD, Stafford RJ. Dynamic chemical shift imaging for image-guided thermal therapy: analysis of feasibility and potential. Med Phys. 2008; 35(2):793–803. [PubMed: 18383702]
32. Koehl P. Linear Prediction Spectral Analysis of NMR Data. Progress in Nuclear Magnetic Resonance Spectroscopy. 1999; 34:257–299.
33. Amindavar H, Reza AM. A New Simultaneous Estimation of Directions of Arrival and Channel Parameters in a Multipath Environment. IEEE Transactions on Signal Processing. 2005; 53(2): 471–483.
34. Kanayama S, Kuhara S, Satoh K. In vivo rapid magnetic field measurement and shimming using single scan differential phase mapping. Magn Reson Med. 1996; 36(4):637–642. [PubMed: 8892219]
35. Wang ZJ, Lian L, Chen Q, Zhao H, Asakura T, Cohen AR. 1/T2 and magnetic susceptibility measurements in a gerbil cardiac iron overload model. Radiology. 2005; 234(3):749–755. [PubMed: 15734931]
36. Wang ZJ, Li S, Haselgrove JC. Magnetic resonance imaging measurement of volume magnetic susceptibility using a boundary condition. J Magn Reson. 1999; 140(2):477–481. [PubMed: 10497053]
37. Villeneuve JP, Bilodeau M, Lepage R, Cote J, Lefebvre M. Variability in hepatic iron concentration measurement from needle-biopsy specimens. J Hepatol. 1996; 25(2):172–177. [PubMed: 8878778]
38. McCarville MB, Hillenbrand CM, Loeffler RB, Smeltzer MP, Song R, Li CS, Hankins JS. Comparison of whole liver and small region-of-interest measurements of MRI liver R2* in children with iron overload. Pediatr Radiol. 2010; 40(8):1360–1367. [PubMed: 20333511]
39. Schenck JF. The role of magnetic susceptibility in magnetic resonance imaging: MRI magnetic compatibility of the first and second kinds. Med Phys. 1996; 23(6):815–850. [PubMed: 8798169]
40. Fischer R, Harmatz P, Nielsen P. Does liver biopsy overestimate liver iron concentration? Blood. 2006; 108(5):1775–1776. author reply 1776. [PubMed: 16926297]

41. Fischer R, Piga A, Harmatz P, Nielsen P. Monitoring long-term efficacy of iron chelation treatment with biomagnetic liver susceptometry. Ann N Y Acad Sci. 2005; 1054:350–357. [PubMed: 16339683]

42. Butensky E, Fischer R, Hudes M, Schumacher L, Williams R, Moyer TP, Vichinsky E, Harmatz P. Variability in hepatic iron concentration in percutaneous needle biopsy specimens from patients with transfusional hemosiderosis. Am J Clin Pathol. 2005; 123(1):146–152. [PubMed: 15762291]

43. Beilby JP, Prins AW, Swanson NR. Determination of hepatic iron concentration in fresh and paraffin-embedded tissue. Clin Chem. 1999; 45(4):573–574. [PubMed: 10102921]

44. Lu W, Yu H, Shimakawa A, Alley M, Reeder SB, Hargreaves BA. Water-fat separation with bipolar multiecho sequences. Magn Reson Med. 2008; 60(1):198–209. [PubMed: 18581362]

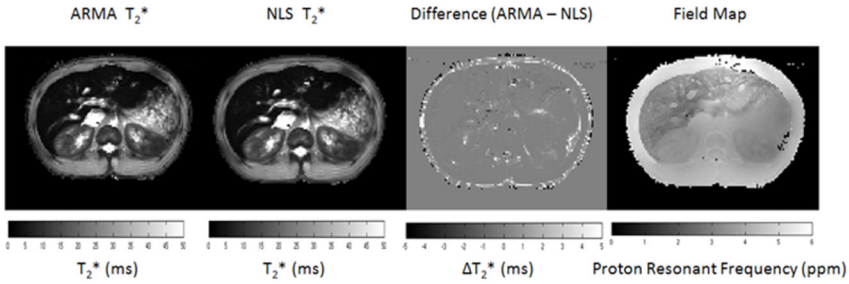

Figure 1.
ARMA and non-linear least squares (NLS) T_2* maps. There is little difference in the values particularly in the liver. Differences are mostly seen in the adipose tissue. The field map indicates a shift in the PRF in the liver, which is indicative of iron overload.

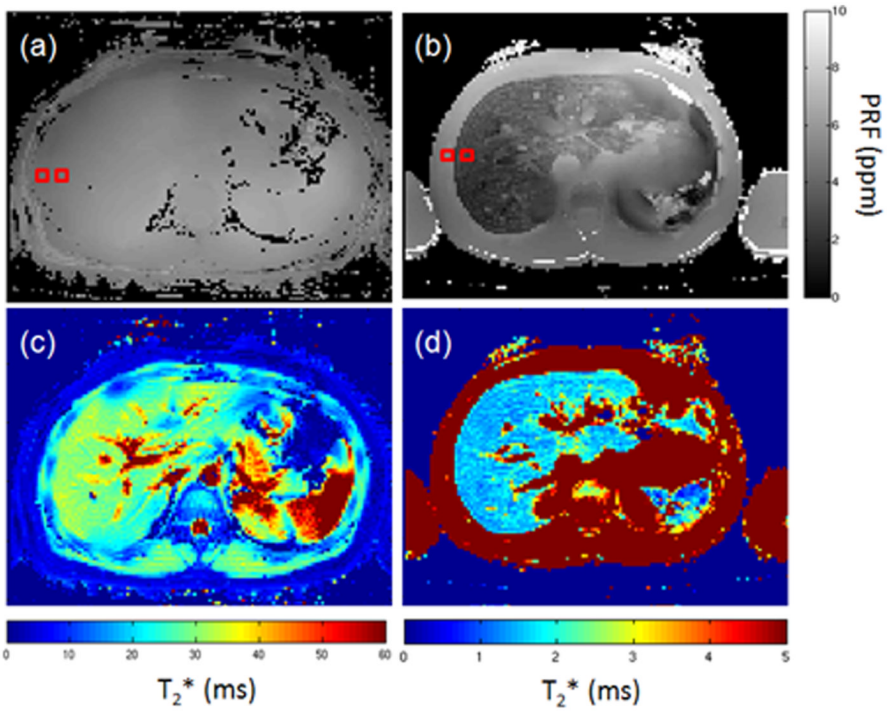

Figure 2.

ARMA field and R_2* maps in a volunteer and patient. The top (panels (a) and (b)) and bottom (panels (c) and (d)) images are the field maps and T_2* maps, respectively. The left images (panels (a) and (c)) are from a normal volunteer (R_2*=35.9 ± 5.6 Hz). Note that it is difficult to distinguish the liver and surrounding tissue in the field maps. The images on the right (panels (b) and (d)) belong to a patient with a whole-liver R_2* LIC estimated as 16.5 ± 2.2 mg Fe/g dry weight liver. The susceptibility was measured as $3.20\times10^{-6} \pm 0.43\times10^{-6}$ between the right lateral side of the liver and the adjacent soft tissue. This susceptibility was approximately 27.8 higher than that of the field map of the volunteer ($1.15\times10^{-7} \pm 0.05\times10^{-7}$). The red squares are the ROIs for susceptibility and R_2* measurements.

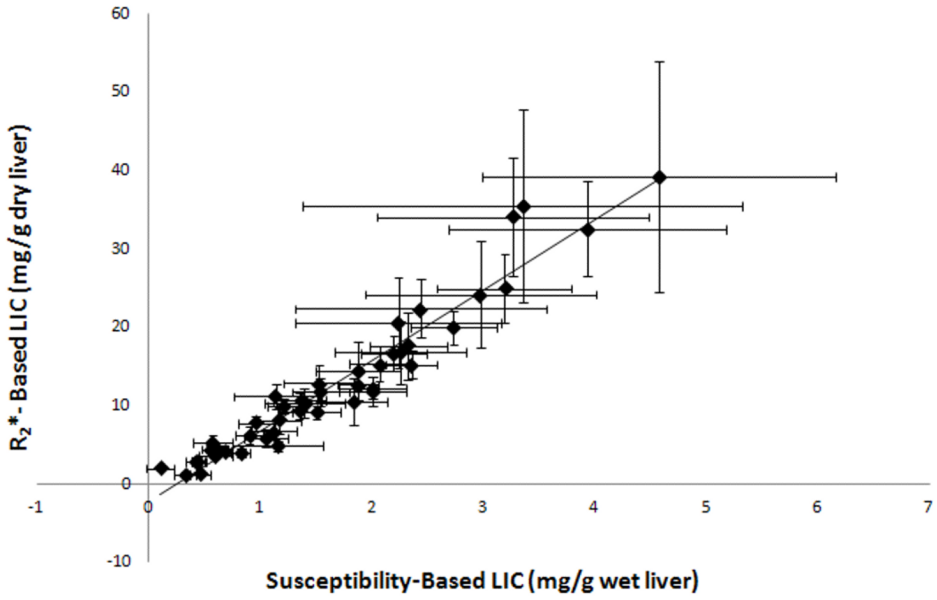

Figure 3.

Plot of the iron concentration from the ROI-based R_2* method and susceptibility method. The dry liver iron concentration from the R_2* method was highly correlated to the wet-liver weight from the susceptibility method (R^2=0.94). The slope of the regression line was 8.99 ± 0.15 mg Fe/g dry liver per mg Fe/ml of wet liver. The intercept was measured as -2.38± 0.29 mg Fe/g dry liver.

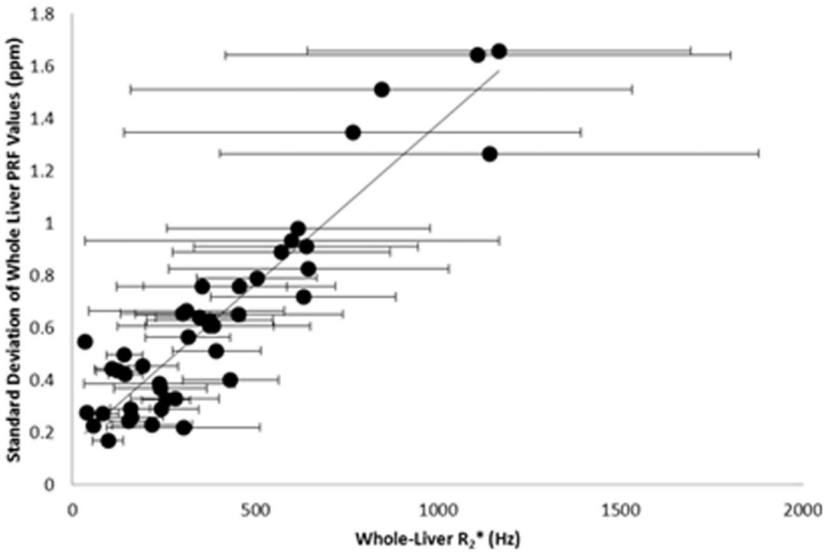

Figure 4.

The variation of PRF values was correlated to the whole-liver mean R_2* value. The slope was 0.0012 ± 0.0005 ppm/Hz with an intercept of 0.15 ± 0.26 ppm (R^2=0.85). This indicates that an iron-overloaded liver will cause increased field inhomogeneity across the liver.

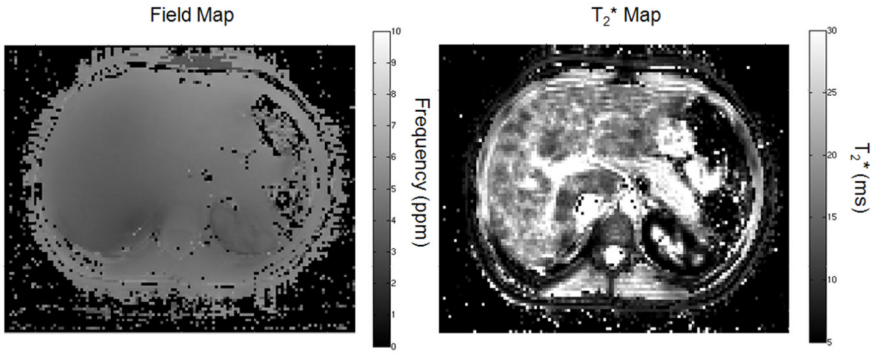

Figure 5.

This case from a patient with multiple blood transfusions underscores how the field map can provide complementary data to distinguish iron overload and other processes such as fibrosis. A patient was scanned with the mGRE acquisition, which showed heterogeneity in the liver on the T_2* map. The T_2* values as low as 3 ms could indicate increased LIC. However, the field map showed a 0.24 ppm frequency shift corresponding to a normal LIC of 0.29 mg Fe/g wet liver demonstrating that this may not be an iron-overload process. This was confirmed by biopsy that showed fibrosis with minimal fat and only traces of iron.